Time-lapse inverse scattering theory

Musa Maharramov and Biondo L. Biondi

ABSTRACT

"Time-lapse inverse scattering theory" that we introduce in this paper focuses on recovering changes in physical models without accurate knowledge of model backgrounds. More specifically, we study the feasibility of recovering low and high-wavenumber components of model perturbation using the traditional Born and Rytov scattering approximations, and establish a connection between the Rytov approximation and phase-only full-waveform inversion (FWI). We provide a theoretical justification for applying regularized simultaneous time-lapse FWI to problems of applied seismology. We demonstrate the method's sensitivity to realistic production effects in seismic data, and its stability with respect to inaccurate starting models.

INTRODUCTION

This work is dedicated to developing a systematic theory for solving *time-lapse* inversion problems that we subsequently refer to as *time-lapse inverse theory*. The term "time-lapse" relates to separate observations of physical phenomena taken at discrete time intervals. Inverse time-lapse theory concerns itself with estimating or *inverting* changes in the underlying physical models from such discrete observations.

Problems of time-lapse or "4D" seismic imaging and reservoir geomechanics that arise in Petroleum Industry(Johnston, 2013; Biondi et al., 1996) provide important applications for the developed theory, and are the primary target of our work as an exploration geophysicists. However, many fundamental concepts, constructs and ideas presented in this work, as well some mathematical, algorithmic and computational byproducts of this research, are applicable beyond the limits of exploration seismology and reservoir geomechanics. We envisage ubiquitous applications of these results to diverse problems of acoustic and electromagnetic inverse scattering, imaging sciences and large-scale numerical optimization. Exploration geophysicists are the primary and key audience of this work, however, we have attempted to make our narrative accessible to specialists in applied mathematics and mathematical physics. Although a considerable part of this work is dedicated to providing a robust and systematic theoretical background for the proposed inversion techniques, we have structured the material in such a way that a motivated practitioner can go straight to examples and case studies, as well as the nuts and bolts of specific algorithms as required for immediate practical application.

If we think of seismic time-lapse analysis as an estimation of *changes* in subsurface model parameters[1] that occurred between two separate seismic experiments, the "inverse time-lapse theory" can be simply regarded as a subset of the inverse acoustic scattering theory. Indeed, classical scattering theory addresses the problem of estimating properties of a "scatterer"—a perturbation in the background model—from incident and scattered wave fields. If production-induced subsurface changes are regarded as a penetrable scatterer, then the 4D analysis simply becomes a problem of inverse scattering theory. If so, why develop a new "time-lapse" inverse theory?

The answer is quite simple. In practical time-lapse applications of exploration geophysics and beyond, the background model is not known accurately. Moreover, errors in our best estimates of the background model can be of the same magnitude as, or even exceed, the time-lapse effects that we seek to estimate. Is it even possible to estimate time-lapse changes when their magnitudes can be easily masked by the effects of measurement noise or errors in the background model? The main product of this research is a systematic theory of inverting small (and spatially bounded) time-lapse changes from noisy and insufficient observations. The proposed "time-lapse inverse theory" differs from inverse theory by placing emphasis on accurate estimation of *relative model changes* while ignoring errors in the background and perturbed models. We provide a toolkit of robust inversion techniques for accurate inversion of time-lapse changes, and demonstrate them on a synthetic example.

Effective methodologies exist for detecting production-induced reflectivity changes and translating them into impedance changes due to fluid substitution or reservoir compaction (Johnston, 2013; Biondi et al., 1996). However, resolving strains in the overburden from seismic data currently requires extraction of time shifts from cross-equalized surveys and mapping the estimated time-strains into the overburden (Rickett et al., 2007). Therefore, we make the primary emphasis of this paper achieving automated recovery of long-wavelength small-magnitude changes of the subsurface acoustic velocities caused by overburden dilation. Maharramov and Biondi (2014d, 2015a) proposed a method for a simultaneous multi-scale inversion of both low and high-wavenumber production anomalies. We demonstrate a hierarchical approach to multi-scale inversion for the recovery of both long-wavelength blocky overburden anomalies and short-wavelength reservoir effects.

EARLIER WORK

Prevalent practice in time-lapse seismic processing relies on picking time displacements and changes in reflectivity amplitudes between migrated baseline and monitor images, and converting them into impedance changes and subsurface deformation (Johnston, 2013). This approach requires a significant amount of manual interpretation and quality control. One alternative approach uses the high-resolution power of full-waveform inversion (Sirgue et al., 2010) to reconstruct production-induced

[1]as a result of petroleum production, fluid injection or environmental phenomena

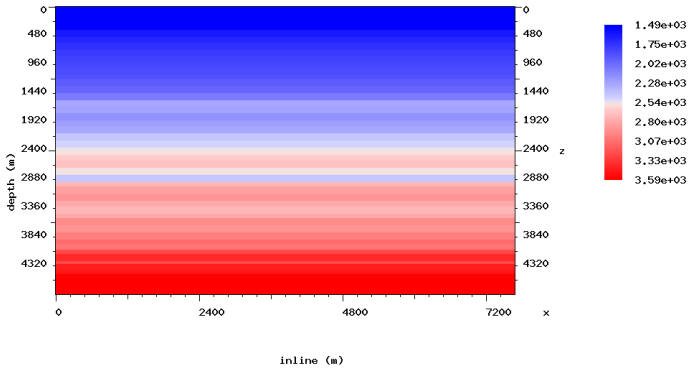

Figure 1: The true baseline model. We chose a flat reflector model to study the sensitivity of FWI of short-offset reflection data to small velocity perturbation in the overburden. [**ER**]

changes from wide-offset seismic acquisitions (Routh et al., 2012; Zheng et al., 2011; Asnaashari et al., 2012; Raknes et al., 2013; Maharramov and Biondi, 2014b; Yang et al., 2014; Maharramov et al., 2015a). However, while potentially reducing the amount of manual interpretation, time-lapse FWI is sensitive to repeatability issues (Asnaashari et al., 2012), with both coherent and incoherent noise potentially masking important production-induced changes. The joint time-lapse FWI proposed by Maharramov and Biondi (2013, 2014b) addressed repeatability issues by joint inversion of multiple vintages with model-difference regularization based on the L_2-norm and produced improved results when compared to the conventional time-lapse FWI techniques. Maharramov et al. (2015b) extended this joint inversion approach to include edge-preserving total-variation (TV) model-difference regularization. The new method was shown to achieve a dramatic improvement over alternative techniques by significantly reducing oscillatory artifacts in the recovered model difference for synthetic data with repeatability issues. Originally, the method was envisaged for applications to large-offset datasets where FWI is traditionally strong. However, Maharramov and Biondi (2015b); Maharramov et al. (2015a) applied this method in a Gulf of Mexico case study to resolving small $(1-2\%)$ production-induced velocity changes associated with overburden dilation. The approach used phase-only FWI of reflection-only data with 5 km maximum offset and target reflectors at about 4 km depth.

While both synthetic and field data experiments involving joint time-lapse FWI with a model-difference regularization indicate robustness and broad applicability of the proposed technique, a detailed theoretical analysis of the joint inversion method is highly desirable for understanding its strengths and limitations.

THEORY

Assuming known background slowness $s(\mathbf{x}), \mathbf{x} \in \mathbb{R}^3$ and a slowness perturbation $\delta s(\mathbf{x})$, the total wavefield component $u(\mathbf{x})$ for frequency ω satisfies the Helmholtz

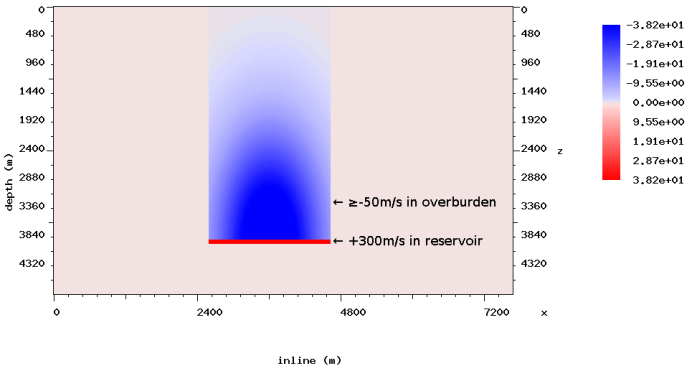

Figure 2: The true model difference is a combination of a positive +300 m/s velocity change in a target reflector at a depth of 3900 m, and a negative velocity change in the overburden above the reflector, peaking at −50 m/s. In this work we investigate the sensitivity of simultaneous time-lapse FWI to small and blocky velocity changes in the overburden. [**ER**]

equation

$$\left[\Delta + \omega^2(s(\mathbf{x}) + \delta s(\mathbf{x}))\right] u(\mathbf{x}) \;=\; -f(\mathbf{x}),\; \mathbf{x} \in D \subset \mathbb{R}^3, \tag{1}$$

where $f(\mathbf{x})$ is the seismic source component for frequency ω. The total wavefield is the sum of incident and scattered wavefields

$$u(\mathbf{x}) \;=\; u_I(\mathbf{x}) \;+\; u_S(\mathbf{x}), \tag{2}$$

where the incident wavefield u_I satisfies the Helmoholtz equation with the unperturbed slowness:

$$\left[\Delta + \omega^2 s(\mathbf{x})\right] u_I(\mathbf{x}) \;=\; -f(\mathbf{x}). \tag{3}$$

Note for well-posedness of (1) and (3) we need to impose an additional condition on the solution, such as the Sommerfeld radiation condition for a homogeneous medium (Colton and Kress, 1998). Physically, such a condition requires that the total field be outgoing at infinity. We will assume that equations (1) and (3) are solved in a domain $D \subset \mathbf{R}^3$, and absorbing boundary conditions (Engquist and Majda, 1977) are applied along the domain boundary, ensuring outgoing propagation of the wavefields.

For time-lapse problems we consider slowness perturbations $\delta s(\mathbf{x})$ with support wholly contained in the interior of D. If $G(\mathbf{x}, \mathbf{y})$ is Green's function for the unperturbed Helmholtz equation (3) in D and absorbing boundary conditions, then equation (1) is equivalent to the Lippmann-Schwinger integral equation

$$u_S(\mathbf{x}, \mathbf{y}) \;= -\,\omega^2 \int_D G(\mathbf{x}, \mathbf{y}) \delta s(\mathbf{y}) \left[u_I(\mathbf{y}) + u_S(\mathbf{y})\right] d\mathbf{y}, \tag{4}$$

or, equivalently,

$$u_S(\mathbf{x}, \mathbf{y}) \;= -\,\omega^2 \int_{\text{supp}\,\delta s} G(\mathbf{x}, \mathbf{y}) \delta s(\mathbf{y}) \left[u_I(\mathbf{y}) + u_S(\mathbf{y})\right] d\mathbf{y}. \tag{5}$$

The incident wavefield $u_I(\mathbf{x})$ in (4),(5) is assumed known.

Our method does not rely on solving (5). However, we will briefly discuss potential advantages of solving Lippmann-Schwinger instead of the Helmholtz equation. Three

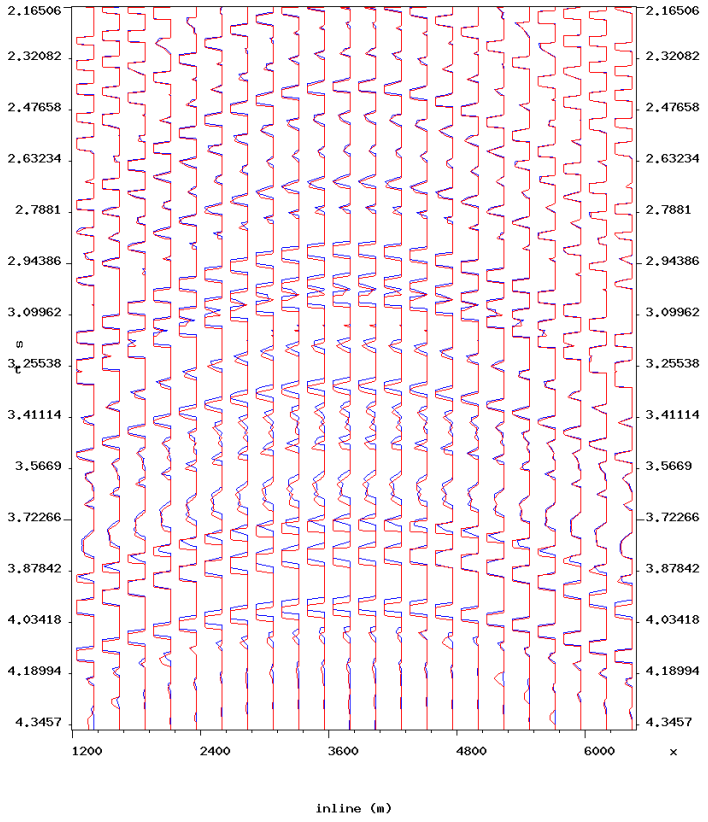

Figure 3: Time shifts observed in common-midpoint gathers centered above the target reservoir (blue is baseline, red is monitor). Travel times of the monitor near-offset reflections traveling through the negative velocity anomaly of Figure 2 are slightly delayed. [**CR**]

advantages of solving (5) for time-lapse problems instead of solving (1) with absorbing boundary conditions are immediately evident. First, it suffices to solve the Lippmann-Schwinger equation in the domain $\operatorname{supp}\delta s$ that in practical applications is much smaller that D (e.g., compaction effects are limited to overburden above producing reservoirs). After discretization, (5) becomes a system of linear equations with a dense modeling operator, and dimension of the model space is determined by the size of $\operatorname{supp}\delta s$ over the computational grid. Second, solution to (5) automatically satisfies absorbing boundary conditions along ∂D because the unperturbed Green's function $G(\mathbf{x},\mathbf{y})$ already satisfies those conditions. Third, once the scattered field is computed inside the support of δs, equation (5) can be used to compute its values outside the perturbation—e.g., at surface receivers.

However, discretization of (5)[2] is a dense linear system, and its numerical properties are highly dependent on the spectral content (smoothness) of δs (Duan and Rokhlin, 2009). "Sparsifying" preconditioners for (5) are an area of active research (see Ying (2015) for homogeneous backgrounds) and merit an investigation as a potentially useful technique for forward modeling of scattered wavefields for spatially bounded perturbations. Another challenge of using (5) is that it explicitly contains Green's function for problem (3). However, spatial boundedness of one of the arguments allows practical application of precomputed Green's functions (Etgen, 2012). In (5) both source and receiver arguments belong to the support of perturbation δs, making use of precomputed Green's functions feasible for compact targets. Computation of the scattered wavefield $u_S(\mathbf{x})$ outside of $\operatorname{supp}\delta s$ can be computationally equally efficient as the wavefield is required only at surface receiver locations.

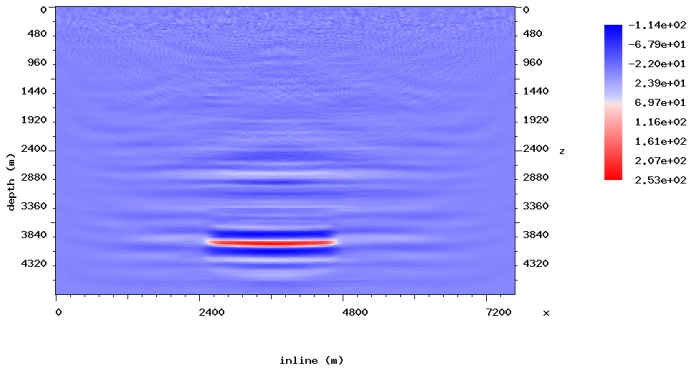

Figure 4: The parallel difference method (Maharramov and Biondi, 2014c) fails to resolve the long-wavelength velocity changes of Figure 2 changes in the overburden, and produces negative short-wavelength artifacts around the target reflector. [**CR**]

Assuming that $\delta s = O(\epsilon)$ where ϵ is a characteristic magnitude of model perturbation, and formally representing the scattered wavefield as a series

$$u_S(\mathbf{x}) \;=\; u_S^{(1)}(\mathbf{x}) \;+\; u_S^{(2)}(\mathbf{x}) \;+\; \ldots, \tag{6}$$

where

$$u_S^{(i)}(\mathbf{x}) \;=\; O(\epsilon^i), \tag{7}$$

[2]using quadratures similar to Duan and Rokhlin (2009) for handling singularities at $\mathbf{x}=\mathbf{y}$

we obtain

$$\begin{aligned} u_S^{(1)}(\mathbf{x}) &= -\omega^2 \int_{\text{supp}\,\delta s} G(\mathbf{x},\mathbf{y})\delta s(\mathbf{y}) u_I(\mathbf{y}) d\mathbf{y}, \\ u_S^{(i+1)}(\mathbf{x}) &= -\omega^2 \int_{\text{supp}\,\delta s} G(\mathbf{x},\mathbf{y})\delta s(\mathbf{y}) u_S^{(i)}(\mathbf{y}) d\mathbf{y},\ i=0,1,\dots \end{aligned} \tag{8}$$

From (8) we immediately see limitations of the Born series (6) in relating the diffracted wavefield $u_S(\mathbf{x})$ to $\delta s(\mathbf{x})$ for long-wavelength small-magnitude model perturbations. Indeed, assuming without a loss of generality, homogeneous background $s(\mathbf{x}) = s_0$ and constant and finite δs, we have

$$G(\mathbf{x},\mathbf{y}) = \frac{\exp(i\omega s_0|\mathbf{x}-\mathbf{y}|)}{4\pi|\mathbf{x}-\mathbf{y}|}. \tag{9}$$

Incident plane wave propagating along axis x^1 is given by

$$u_I(\mathbf{x}) = \exp(i\omega s_0 x^1). \tag{10}$$

For a sufficiently small $\text{diam}\,(\text{supp}\,\delta s) \ll x^1$ the denominator of (9) is asymptotically a constant factor if $\mathbf{y} \in \text{supp}\,\delta s$, and from (8) we obtain

$$\begin{aligned} u_S^{(1)}(x^1,0,0) &\approx -\frac{\delta s\cdot\omega^2}{4\pi x^1}\int_{\text{supp}\delta s\cap\mathbb{R}^1} \exp(i\omega s_0(x^1-y^1))\exp(i\omega s_0 y^1)dy^1 \\ &= -\frac{L\cdot\delta s\cdot\omega^2}{4\pi x^1}\exp(i\omega s_0 x^1), \end{aligned} \tag{11}$$

where

$$L = |\text{supp}\delta s\cap\mathbb{R}^1(x^1)|, \tag{12}$$

is the length of model perturbation along axis $\mathbb{R}^1(x^1)$. Equation (11) means that the first-order Born scattering under our assumptions only affects the amplitude but not the phase of the scattered wavefield. Indeed, phase changes accumulate in (6) through the effect of the denominator in (9), requiring exponentially many terms to account for a phase delay or advance in the scattered (transmitted) wavefield. However, transmission through a constant perturbation δs of length L would cause a phase change proportional to $L\delta s$, therefore any technique based on truncated Born scattering would be suboptimal for relating large-wavelength, or "blocky", velocity perturbations to measured scattered wavefields. This is a well-known limitation of the diffraction tomography (Wu and Toksoz, 1987) that is inherited by full-waveform inversion using L_2 misfit (Fichtner, 2011). On the other hand, Born series is a very good scattering approximation for small-wavelength, large-amplitude perturbations as, again, demonstrated by equation (11) (compare with Slaney et al. (1984)).

Rytov scattering series (Ishimaru, 1999) based on asymptotic phase expansion of the scattered wavefield linearly relates phase changes and magnitudes of the slowness change in first approximation, as does the initial approximation of full-waveform

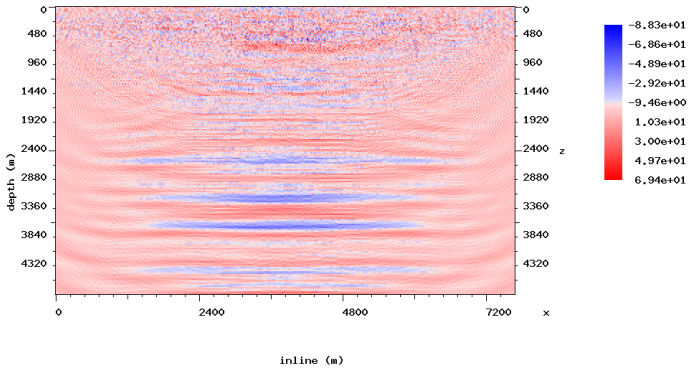

Figure 5: The cross-updated FWI method (Maharramov and Biondi, 2014c) cross-equalizes the baseline and monitor model but still fails to resolve the long-wavelength overburden changes of Figure 2. [**CR**]

inversion of phase differences (Fichtner, 2011). Moreover, in time-lapse problems of inverting long-wavelength small-magnitude model perturbations, Rytov inverse scattering (and phase-only FWI) are less sensitive to errors in the background model.

Indeed, assuming for simplicity, but without a loss of generality, a constant background s_0 and constant finite perturbation δs, the phase change for transmitted a plane wave traveling through a perturbation δs of characteristic dimension L is approximately proportional to $L\delta s/s_0$. For significant phase changes phase wraps around 2π, and this happens when the phase delay is a multiple of the incident wavelength. Fitting peaks and trough of the modeled and observed scattered wavefields (ignoring the amplitude information) then results in ambiguity of the total phase change: phase change can be resolved only within an integer multiple of incident wavelengths. This results in a well known phenomenon of cycle skipping in FWI: unless the FWI starting slowness model is known within a full wavelength of the incident wave, the model cannot be resolved from signal phase information alone.

However, for time-lapse problems phase change due to a compact velocity anomaly is only a fraction of the wavelength. Indeed, translating to the time domain, time shifts due to dilation in overburden peak at about 10 ms (Rickett et al., 2006; Maharramov and Biondi, 2015b; Maharramov et al., 2015a)—i.e., about a third of the period for a 30 Hz signal (see Figure 3). Therefore, phase changes (equivalently, time delays) of scattered wavefields for small-magnitude long-wavelength perturbations that are of interest for us can still be translated into slowness changes, albeit errors in the background will result in errors in the estimated slowness perturbation:

$$\delta s_W \;=\; \frac{s_W}{s_0}\delta s, \tag{13}$$

where s_W is the inaccurate background slowness and δs_W is the corresponding estimated slowness perturbation. Equation (13) means that even with a wrong background a qualitative perturbation magnitude information can still be extracted from the scattered wavefield. Note that location of the perturbation is determined by the illumination pattern of incident wavefields. Poor target illumination results in the ambiguity of anomaly characteristic dimension L versus the perturbation magnitude

δs as the two enter in (13) in a product. For example, lack of reflectors above the velocity anomaly results in an ambiguous vertical extent of the anomaly.

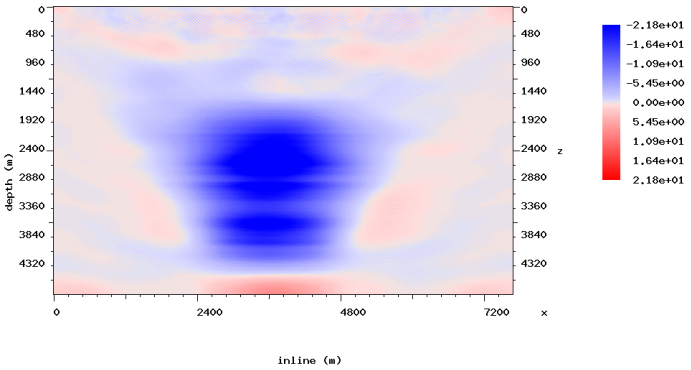

Figure 6: Simultaneous FWI with a total-variation model-difference regularization (Maharramov and Biondi, 2014e) resolves the long-wavelength overburden changes of Figure 2, but underestimates the maximum change, depending on the regularization strength. [**CR**]

To implement a practical time-lapse inversion method using phase-only FWI, we can invert two models (unperturbed baseline and perturbed monitor) simultaneously, imposing a model-difference regularization. The latter is required to create a common "background" model for both inversions making the application of (13) possible. Note that baseline and monitor inversions may still cycle-skip, but the purpose of imposing a model-difference regularization is to ensure that they are either equally accurate or equally inaccurate for wavelengths greater than the characteristic wavelength of the inverted perturbation.

For blocky, long-wavelength anomalies we impose blockiness-promoting total variation regularization (Maharramov and Biondi, 2014e), while for the recovery of short-wavelength features we use L_2 Tikhonov model-difference regularization (Maharramov and Biondi, 2013).

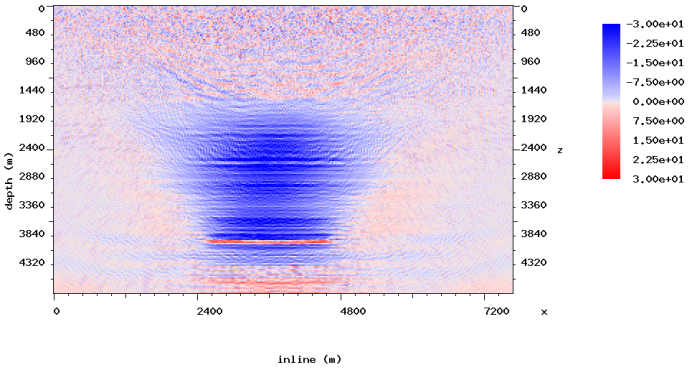

Figure 7: Simultaneous FWI using Tikhonov model-difference regularization, with the long-wavelength inversion of Figure 6 supplied as a prior. Note that such multiscale approach can now resolve the short-wavelength positive-velocity changes of Figure 2. Strong Tikhonov regularization results in underestimated velocity changes within the reservoir but correctly locates the anomalies. [**CR**]

METHOD

Full-waveform inversion is defined as solving the following optimization problem (Tarantola, 1984; Virieux and Operto, 2009)

$$\|\mathbf{Mu}-\mathbf{d}\|_2 \;\rightarrow\; \min, \tag{14}$$

where $\mathbf{M},\mathbf{d}$ are the measurement operator and data, $\mathbf{u}$ is the solution of a forward-modeling problem

$$\mathbf{D}(\mathbf{m})\mathbf{u} \;=\; \phi, \tag{15}$$

where $\mathbf{D}$ is the forward-modeling operator that depends on a model vector $\mathbf{m}$ as a parameter, and ϕ is a source. The minimization problem (14) is solved with respect to either both the model $\mathbf{m}$ and source ϕ or just the model. In the frequency-domain formulation of the acoustic waveform inversion, the forward-modeling equation (15) becomes

$$-\omega^2 u - v^2(x^1,\ldots,x^n)\Delta u \;=\; \phi(\omega,x^1,\ldots,x^n), \tag{16}$$

where ω is a temporal frequency, n is the problem dimension, and v is the acoustic wave propagation velocity. Values of the slowness $s=1/v$ at all the points of the modeling domain constitute the model parameter vector $\mathbf{m}$. The direct problem (16) can be solved in the frequency domain (Virieux and Operto, 2009). The inverse problem (14) is typically solved using a multiscale approach, from low to high frequencies, supplying the output of each frequency inversion to the next step (Fichtner, 2011).

FWI applications in time-lapse problems seek to recover induced changes in the subsurface model using multiple datasets from different acquisition vintages. For two surveys sufficiently separated in time, we call such datasets (and the associated models) *baseline* and *monitor*.

Time-lapse FWI can be carried out by separately inverting the baseline and monitor models (*parallel difference*), or by inverting them sequentially with, e.g., the baseline supplied as a starting model for the monitor inversion (*sequential difference*). Another alternative is to apply the *double-difference* method, with a baseline model inversion followed by a monitor inversion that solves the following optimization problem,

$$\|\,(\mathbf{M}^s_m\mathbf{u}_m-\mathbf{M}^s_b\mathbf{u}_b)-(\mathbf{M}_m\mathbf{d}_m-\mathbf{M}_b\mathbf{d}_b)\,\|_2 \;\rightarrow\; \min, \tag{17}$$

by changing the monitor model (Watanabe et al., 2004; Denli and Huang, 2009; Zheng et al., 2011; Asnaashari et al., 2012; Raknes et al., 2013). The subscripts in equation (17) denote the baseline and monitor surveys, $\mathbf{d}$ denotes the observed data, and the $\mathbf{M}$'s are measurement operators that project the synthetic and field data onto a common grid. The superscript s indicates the measurement operators applied to the modeled data. For phase-only inversion, in all of the subsequent equations, the modeled and observed data differences should be replaced with the corresponding "phase differences"

$$\mathbf{u}\;-\;\mathbf{d} \;\Longrightarrow\; \sin\arg\mathbf{u}\;-\;\sin\arg\mathbf{d}, \tag{18}$$

where arg is the complex argument function of frequency domain wavefields. Note that unlike the traditional phase-only inversion (Fichtner, 2011), we evaluate sine of the phase to avoid phase discontinuities.

In all of these techniques, optimization is carried out with respect to one model at a time, albeit of different vintages at different stages of the inversion. In our method we invert for the baseline and monitor models *simultaneously* by solving either one of the following two optimization problems:

$$\alpha\|\mathbf{M}_b\mathbf{u}_b - \mathbf{d}_b\|_2^2 + \beta\|\mathbf{M}_m\mathbf{u}_m - \mathbf{d}_m\|_2^2 + \tag{19}$$
$$\gamma\|\left(\mathbf{M}_m^s\mathbf{u}_m - \mathbf{M}_b^s\mathbf{u}_b\right) - \left(\mathbf{M}_m\mathbf{d}_m - \mathbf{M}_b\mathbf{d}_b\right)\|_2^2 + \tag{20}$$
$$\alpha_1\|\mathbf{W}_b\mathbf{R}_b(\mathbf{m}_b - \mathbf{m}_b^{\text{PRIOR}})\|_2^2 + \tag{21}$$
$$\beta_1\|\mathbf{W}_m\mathbf{R}_m(\mathbf{m}_m - \mathbf{m}_m^{\text{PRIOR}})\|_2^2 + \tag{22}$$
$$\delta\|\mathbf{WR}(\mathbf{m}_m - \mathbf{m}_b - \Delta\mathbf{m}^{\text{PRIOR}})\|_2^2 \;\rightarrow\; \min, \tag{23}$$

or

$$\alpha\|\mathbf{M}_b\mathbf{u}_b - \mathbf{d}_b\|_2^2 + \beta\|\mathbf{M}_m\mathbf{u}_m - \mathbf{d}_m\|_2^2 + \tag{24}$$
$$\gamma\|\left(\mathbf{M}_m^s\mathbf{u}_m - \mathbf{M}_b^s\mathbf{u}_b\right) - \left(\mathbf{M}_m\mathbf{d}_m - \mathbf{M}_b\mathbf{d}_b\right)\|_2^2 + \tag{25}$$
$$\alpha_1\|\mathbf{W}_b\mathbf{R}_b(\mathbf{m}_b - \mathbf{m}_b^{\text{PRIOR}})\|_1 + \tag{26}$$
$$\beta_1\|\mathbf{W}_m\mathbf{R}_m(\mathbf{m}_m - \mathbf{m}_m^{\text{PRIOR}})\|_1 + \tag{27}$$
$$\delta\|\mathbf{WR}(\mathbf{m}_m - \mathbf{m}_b - \Delta\mathbf{m}^{\text{PRIOR}})\|_1 \;\rightarrow\; \min, \tag{28}$$

with respect to both the baseline and monitor models $\mathbf{m}_b$ and $\mathbf{m}_m$. Problem (19-23) describes time-lapse FWI with L_2 regularization of the individual models (21,22) and model difference (23) (Maharramov and Biondi, 2014c). The second formulation (24-28) involves an L_1-regularization of the individual models and their difference (Maharramov and Biondi, 2014e; Maharramov et al., 2015b). The terms (24) correspond to separate baseline and monitor inversions, the term (25) is the optional double difference term, the terms (26) and (27) are optional separate baseline and monitor inversion regularization terms (Aster et al., 2012), and the term (28) represents regularization of the model difference. In (26)-(28), $\mathbf{R}$ and $\mathbf{W}$ denote regularization and weighting operators respectively, with the subscript denoting the survey vintage where applicable. If $\mathbf{R}$ is the *gradient magnitude* operator

$$\mathbf{R}f(x,y,z) \;=\; \sqrt{f_x^2 + f_y^2 + f_z^2}, \tag{29}$$

then (26-28) become *total-variation (TV) seminorms*. The latter case is of particular interest in this work as the minimization of the L_1 norm of gradient may promote "blockiness" of the model-difference, potentially reducing oscillatory artifacts (Rudin et al., 1992; Aster et al., 2012).

A joint inversion approach has been applied earlier to the linearized waveform inversion (Ayeni and Biondi, 2012). In Maharramov and Biondi (2013, 2014c,a), a simultaneous full-waveform inversion problem (19,23) was studied with a single model difference L_2 regularization term (23).

An implementation of the proposed simultaneous inversion algorithm requires solving a nonlinear optimization problem with twice the data and model dimensions of problems (14) and (17). The model difference regularization weights $\mathbf{W}$ and, optionally, the prior $\Delta\mathbf{m}^{\text{PRIOR}}$ may be obtained from prior geomechanical information. For example, a rough estimate of production-induced velocity changes can be obtained from time shifts (Hatchell and Bourne, 2005; Barkved and Kristiansen, 2005) and used to map subsurface regions of expected production-induced perturbation, and optionally provide a difference prior. However, successfully solving the L_1-regularized problem (24-25) is less sensitive to choice of the weighting operator $\mathbf{W}$. For example, we show below that the TV-regularization using (29) with $\mathbf{W} = 1$ recovers non-oscillatory components of the model difference, while the L_2 approach would result in either smoothing or uniform reduction of the model difference.

In addition to the fully simultaneous inversion, Maharramov and Biondi (2013, 2014c) proposed and tested a *cross-updating* technique that offers a simple but remarkably effective approximation to minimizing the objective function (19),(23), while obviating the difference regularization and weighting operators $\mathbf{R}$ and $\mathbf{W}$ for problem (19,23). This technique consists of one standard run of the sequential difference algorithm, followed by a second run with the inverted monitor model supplied as the starting model for the second baseline inversion

$$\begin{aligned}\mathbf{m}_{\text{INIT}} \rightarrow &\text{baseline inversion} \rightarrow \text{monitor inversion} \rightarrow \\ &\text{baseline inversion} \rightarrow \text{monitor inversion},\end{aligned} \tag{30}$$

and computing the difference of the latest inverted monitor and baseline models. Process (30) can be considered as an approximation to minimizing (19) and (23) because non-repeatable footprints of both inversions are propagated to both models, canceling out in the difference. Both the simultaneous inversion and cross-updating minimize the model difference by tackling model artifacts that are in the null space of the Fréchet derivative of the forward modeling operatorss. The joint inversion minimizes the effect of such artifacts on the model difference by either minimizing the model difference term (23) in the simultaneous inversion, or by propagating these artifacts to both models in cross-updating (30). Note that this process is not guaranteed to improve the results of the baseline and monitor model inversions but was only proposed for improving the model difference. Maharramov and Biondi (2014c,a) demonstrated a significant improvement of model difference recovery by both the L_2-regularized target-oriented simultaneous inversion and cross-updating compared to the parallel, sequential and double difference techniques. The simultaneous inversion and cross-updating yielded qualitatively similar results within the inversion target. Maharramov et al. (2015c) studied the regularized double-difference inversion (25,28).

NUMERICAL EXPERIMENTS AND DISCUSSION

Our previous work (Maharramov and Biondi, 2014e,b) has demonstrated effective recovery of blocky velocity anomalies from long-offset acquisitions in the presence of

noise and repeatability issues. In this work we demonstrate the recovery of blocky anomalies in the more challenging case of phase-only inversion of narrow-offset reflection data. Conceptually our synthetic example is similar to the earlier field data case study of Maharramov and Biondi (2015b); Maharramov et al. (2015a).

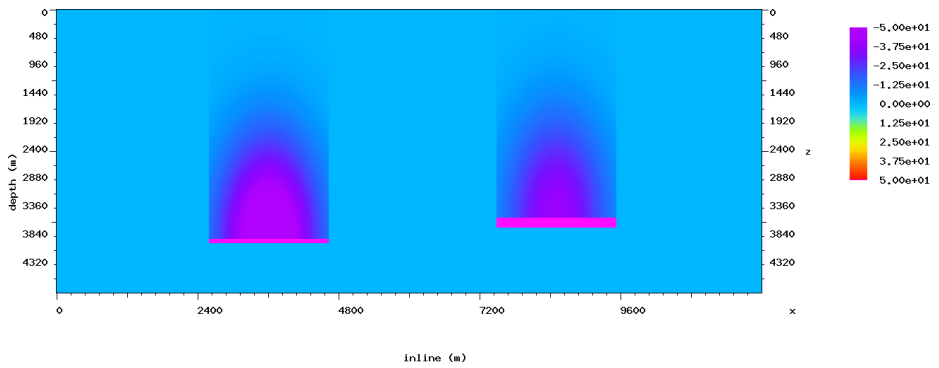

Figure 8: True model difference for demonstrating the inversion of multiple overburden anomalies. [**ER**]

As a baseline model we use the flat reflector model of Figure 1. The target reflector (reservoir) is located at a depth of 3900 m, the monitor (perturbed) model has two velocity anomalies–a positive +300 m/s change due to compaction and fluid substitution within the reservoir, and a blocky negative velocity change in the overburden above the reservoir, peaking at −50 m/s (see Figure 2). No physical reflector movement is prescribed.

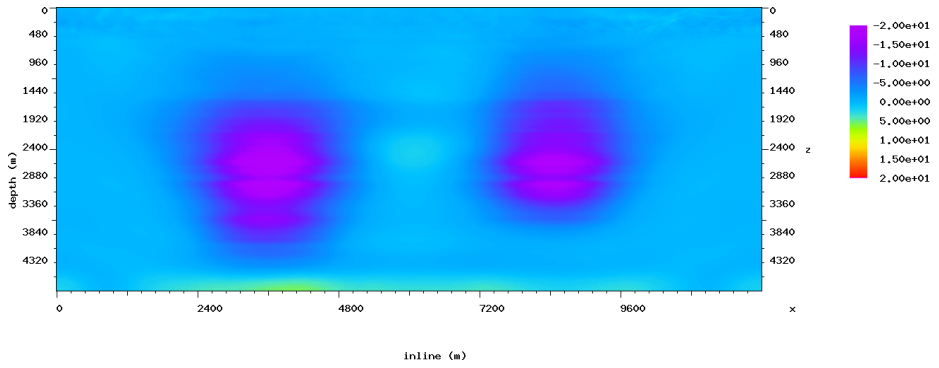

Figure 9: Inversion of the two long-wavelength overburden anomalies of Figure 8 using simultaneous time-lapse FWI with total-variation model-difference regularization. [**CR**]

For generating synthetic data we used a towed streamer acquisition geometry with the maximum offset of 5 km. The results of parallel difference and cross-updating are shown in Figures 4 and 5. Note that neither result succeeds in recovering the blocky anomaly. The FWI starting model used in these experiments was a smoothed true model, using a 720 m smoothing window.

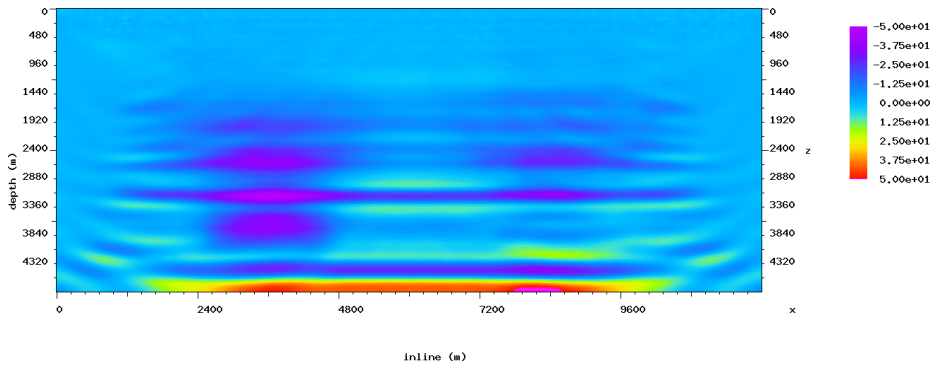

Figure 10: Inversion of the two long-wavelength overburden anomalies of Figure 8 starting from a bad initial model and using weak regularization (a small regularization parameter). FWI cycle skipped, and the baseline and monitor inversion diverged, contaminating the difference with cycle-skipping artifacts. [**CR**]

The result of simultaneous inversion with a total-variation model-difference regularization is shown in Figure 6. The result is qualitatively accurate although peak magnitudes are underestimated due to regularization. To assess the effectiveness of our inversion, in Figures 12(a) and 13(b) we show monitor images migrated using the true monitor and true baseline models, respectively. Note that the overestimated velocities in the overburden result in a downward reflector shift in Figure 13(b). However, migrating the monitor data using the sum of the baseline model and the *inverted* blocky anomaly of Figure 6 results in the image of Figure 13(a): the downward shift of reflectors in the overburden is now significantly reduced.

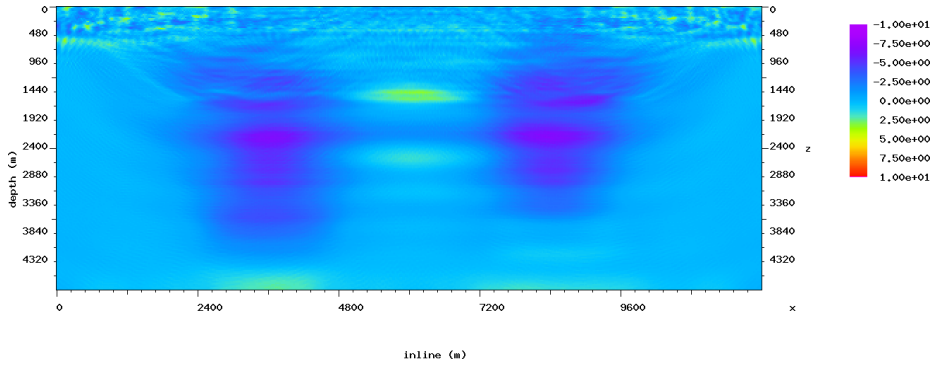

Figure 11: Inversion of the two long-wavelength overburden anomalies of Figure 8 starting from a bad initial model but using stronger regularization (a larger regularization parameter). FWI still cycle skipped, however, the strong model-difference regularization kept baseline and monitor within the characteristic wavelength of the overburden anomalies. The resulting model difference inversion is qualitatively accurate (compare with Figure 9), albeit stronger regularization has resulted in underestimated velocity magnitudes. [**CR**]

To recover the short-wavelength changes within the reservoir, we supplied the

result of Figure 6 as a model-difference prior to inversion (19,23). Note that the resulting model features both long and short-wavelength velocity perturbations. The reservoir perturbation is underestimated due to strong regularization. Maharramov and Biondi (2015a) discuss a regularization scheme for multi-scale inversion that honors true model magnitudes.

And finally, Figures 8 and 9 demonstrate recovery of two separate overburden anomalies. In both cases FWI start from a smoothed true velocity. The result of starting FWI with a wrong velocity resulting in cycle-skipping is shown in Figure 10. We deliberately used a weak regularization parameter at model-difference regularization to demonstrate the effect of diverging baseline and monitor models on the inverted model difference. Figure 11 contains the result of using a stronger TV regularization. As described in the Theory section above, we ensure that the two models cycle-skip "in synchrony" and are still able to qualitatively recover the anomalies, although with strongly underestimated velocities—compare with equation (13).

In this work we provided a theoretical justification for the time-lapse inversion methods of Maharramov and Biondi (2013, 2014e, 2015b) and demonstrated a stable recovery of both short and long-wavelength velocity anomalies form narrow-offset reflection seismic data. We envisage wide-spread application of the simultaneous FWI with model-difference regularization and hierarchical multi-scale inversion in applications ranging from applied geophysics to electromagnetic and optical scattering.

ACKNOWLEDGEMENTS

The authors would like to thank Stewart A. Levin and Mark A. Meadows for a number of useful discussions, and the affiliate members of Stanford Exploration Project for their support.

REFERENCES

Asnaashari, A., R. Brossier, S. Garambois, F. Audebert, P. Thore, and J. Virieux, 2012, Time-lapse imaging using regularized FWI: A robustness study: 82nd Annual International Meeting, SEG, Expanded Abstracts, doi:10.1190/segam2012-0699.1, 1–5.

Aster, R., B. Borders, and C. Thurber, 2012, Parameter estimation and inverse problems: Elsevier.

Ayeni, G. and B. Biondi, 2012, Time-lapse seismic imaging by linearized joint inversion—A Valhall Field case study: 82nd Annual International Meeting, SEG, Expanded Abstracts, doi:10.1190/segam2012-0903.1, 1–6.

Barkved, O. and T. Kristiansen, 2005, Seismic time-lapse effects and stress changes: Examples from a compacting reservoir: The Leading Edge, **24**, no. 12, 1244–1248.

Biondi, B., C. Deutsch, R. Gundes, D. Lumley, G. Mavko, T. Mukerji, J. Rickett,

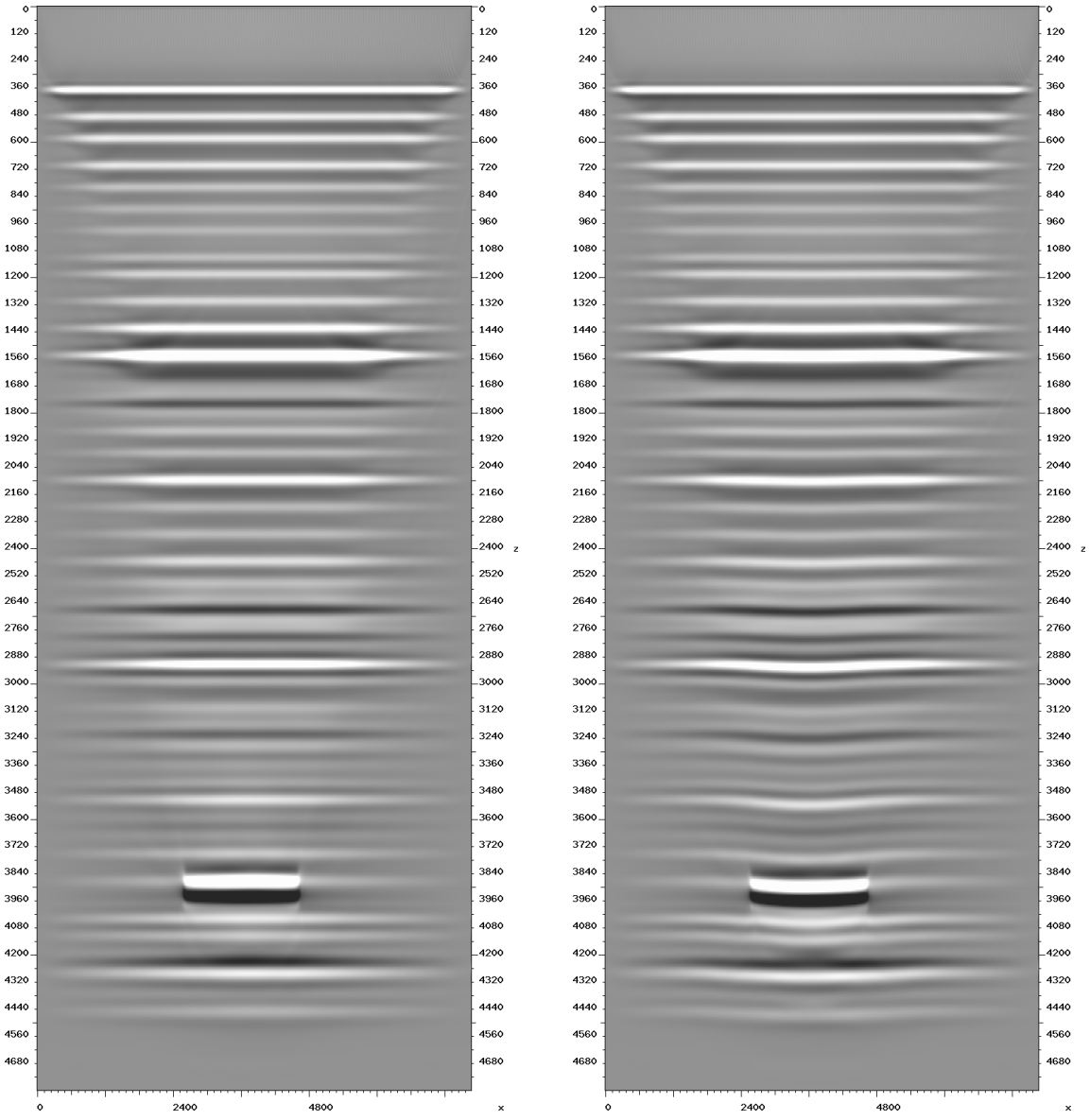

Figure 12: (a) True monitor image. (b) Monitor migrated using the baseline velocity model. Note that overestimated velocity in the overburden results in a downward reflector shift in the right image. [**CR**]

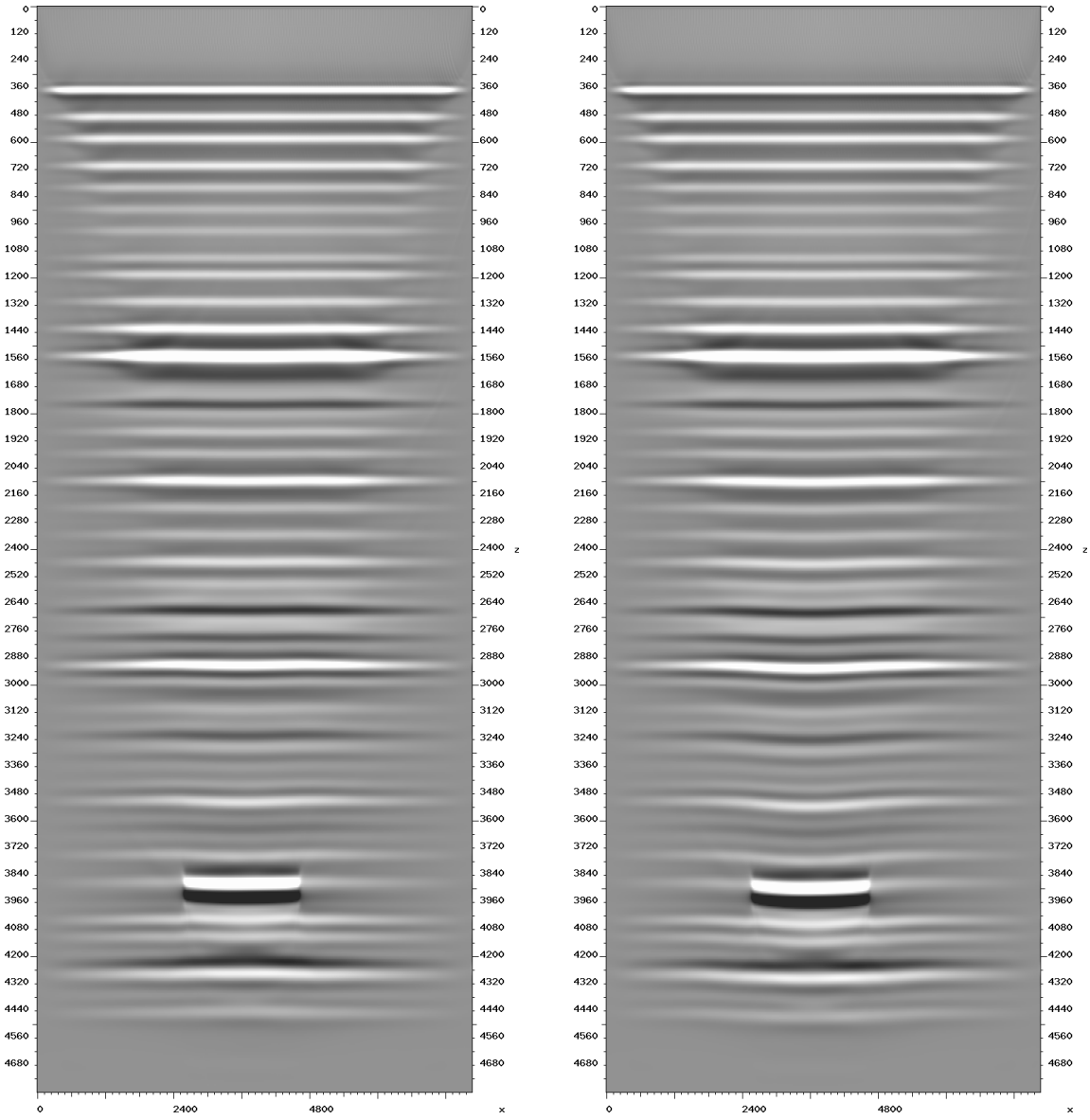

(a) (b)

Figure 13: (a) Monitor image migrated using the sum of the baseline model and inverted model difference of Figure 6. (b) Monitor migrated using the baseline velocity model. Note that reflector shift in the overburden has been significantly reduced in the left image. [**CR**]

and M. Thiele, 1996, Reservoir monitoring: A multidisciplinary feasibility study: 66th Annual International Meeting, SEG, Expanded Abstracts, 1775–1778.

Colton, D. and R. Kress, 1998, Inverse acoustic and electromagnetic scattering theory: Springer.

Denli, H. and L. Huang, 2009, Double-difference elastic waveform tomography in the time domain: 79th Annual International Meeting, SEG, Expanded Abstracts, 2302–2306.

Duan, R. and V. Rokhlin, 2009, High-order quadratures for the solution of scattering problems in two dimensions: J. Comput. Phys., **228**, 2152–2174.

Engquist, B. and A. Majda, 1977, Absorbing boundary conditions for the numerical simulation of waves: Math. Comp., **31**, 629–651.

Etgen, J. T., 2012, 3d wave equation kirchhoff migration: SEG Technical Program Expanded Abstracts 2012, 1–5.

Fichtner, A., 2011, Full seismic modeling and inversion: Springer.

Hatchell, P. and S. Bourne, 2005, Measuring reservoir compaction using time-lapse timeshifts: 75th Annual International Meeting, SEG, Expanded Abstracts, 2500–2503.

Ishimaru, A., 1999, Wave propagation and scattering in random media: Academic Press.

Johnston, D., 2013, Practical applications of time-lapse seismic data: Society of Exploration Geophysicists.

Maharramov, M. and B. Biondi, 2013, Simultaneous time-lapse full waveform inversion: SEP Report, **150**, 63–70.

———, 2014a, Joint 4DFWI with model-difference regularization. SEG-AGU summer research workshop: SEG-AGU Summer Research Workshop. Advances in Active+Passive "Full Wavefield" Seismic Imaging: From Reservoirs to Plate Tectonics.

———, 2014b, Joint full-waveform inversion of time-lapse seismic data sets: 84th Annual Meeting, SEG, Expanded Abstracts, 954–959.

———, 2014c, Joint full-waveform inversion of time-lapse seismic data sets: SEP Report, **152**, 19–28.

———, 2014d, Multi-model full-waveform inversion: SEP Report, **155**, 187–192.

———, 2014e, Robust joint full-waveform inversion of time-lapse seismic datasets with total-variation regularization: SEP Report, **155**, 199–208.

———, 2015a, Multi-scale inversion of subsurface velocity models using cartoon-texture decomposition: SIAM Conference on Mathematical and Computational Issues in the Geosciences, MS2 Full Waveform Inversion I: Algorithms and Performance.

———, 2015b, Resolving the effects of production-induced overburden dilation using simultaneous TV-regularized time-lapse fwi: SEP Report, **158**, 1–10.

Maharramov, M., B. Biondi, and M. Meadows, 2015a, Simultaneous tv-regularized time-lapse fwi with application to field data: SEG Technical Program Expanded Abstracts 2015, 1236–1241.

Maharramov, M., B. Biondi, and S. Ronen, 2015b, Robust simultaneous time-lapse full-waveform inversion with total-variation regularization of model difference: 77th

EAGE Conference and Exhibition, Extended Abstract, We P3 09.

Maharramov, M., Y. Ma, and B. Biondi, 2015c, Double-difference time-lapse FWI with a total-variation regularization: SEP Report, **158**, 263–270.

Raknes, E., W. Weibull, and B. Arntsen, 2013, Time-lapse full waveform inversion: Synthetic and real data examples: 83rd Annual International Meeting, SEG, Expanded Abstracts, 944–948.

Rickett, J., L. Duranti, T. Hudson, and N. Hodgson, 2006, Compaction and 4D time strain at the Genesis Field: 76th Annual International Meeting, SEG, Expanded Abstracts, 3215–3219.

Rickett, J., L. Duranti, T. Hudson, B. Regel, and N. Hodgson, 2007, 4D time strain and the seismic signature of geomechanical compaction at Genesis: The Leading Edge, **26**, 644–647.

Routh, P., G. Palacharla, I. Chikichev, and S. Lazaratos, 2012, Full wavefield inversion of time-lapse data for improved imaging and reservoir characterization: 82nd Annual International Meeting, SEG, Expanded Abstracts, doi:10.1190/segam2012-1043.1, 1–6.

Rudin, L. I., S. Osher, and E. Fatemi, 1992, Nonlinear total variation based noise removal algorithms: Physica D: Nonlinear Phenomena, **60**, 259–268.

Sirgue, L., O. Barkved, J. Dellinger, J. Etgen, U. Albertin, and J. Kommendal, 2010, Full waveform inversion: The next leap forward in imaging at Valhall: First Break, **28**, no. 4, 65–70.

Slaney, M., A. Kak, and L. Larsen, 1984, Limitations of imaging with first-order diffraction tomography: Microwave Theory and Techniques, IEEE Transactions on, **32**, 860–874.

Tarantola, A., 1984, Inversion of seismic reflection data in the acoustic approximation: Geophysics, **49**, no. 8, 1259–1266.

Virieux, J. and S. Operto, 2009, An overview of full-waveform inversion in exploration geophysics: Geophysics, **74, no.6**, no. 6, WCC1–WCC26.

Watanabe, T., S. Shimizu, E. Asakawa, and T. Matsuoka, 2004, Differential waveform tomography for time-lapse crosswell seismic data with application to gas hydrate production monitoring: 74th Annual International Meeting, SEG, Expanded Abstracts, 2323–2326.

Wu, R. and M. N. Toksoz, 1987, Diffraction tomography and multisource holography applied to seismic imaging: GEOPHYSICS, **52**, 11–25.

Yang, D., A. E. Malcolm, and M. C. Fehler, 2014, Time-lapse full waveform inversion and uncertainty analysis with different survey geometries: 76th EAGE Conference and Exhibition, Extended Abstract, We ELI1 10.

Ying, L., 2015, Sparsifying preconditioner for the lippmann–schwinger equation: Multiscale Modeling & Simulation, **13**, 644–660.

Zheng, Y., P. Barton, and S. Singh, 2011, Strategies for elastic full waveform inversion of timelapse ocean bottom cable (OBC) seismic data: 81st Annual International Meeting, SEG, Expanded Abstracts, 4195–4200.